Structural disorganization of cereal, tuber and bean starches in aqueous ionic liquid at room temperature: role of starch granule surface structure

Ke Zan[†,‡], Jinwei Wang,[†,‡] Fei Ren,[†,‡] Jinglin Yu,[†,‡] Shuo Wang,[§] Fengwei Xie*[¶], Shujun Wang*[,†,‡,⊥]

[†] State Key Laboratory of Food Nutrition and Safety, Tianjin University of Science & Technology, Tianjin 300457, China

[‡] School of Food Science and Technology, Tianjin University of Science & Technology, 300457, China

[§] Tianjin Key Laboratory of Food Science and Health, School of Medicine, Nankai University, Tianjin, 300071, China

[¶]International Institute for Nanocomposites Manufacturing (IINM), WMG, University of Warwick, Coventry, CV4 7AL, United Kingdom

[⊥] College of Biological and Chemical Engineering, Guangxi University of Science and Technology, Liuzhou 545006, China

*** Corresponding authors**

Dr Shujun Wang, Email address: sjwang@tust.edu.cn

Dr Fengwei Xie, Email address: D.Xie.2@warwick.ac.uk

Highlights

- The disorganization of different starches in aqueous ionic liquid (IL) studied
- Granule surface structure key to determining starch dissolution in aqueous IL
- Normal cereal starches show endo-corrosion with complete disorganization within 1.5 h
- Starches with dense layer show exo-corrosion with residual structure at 24 h
- Disorganization accompanied by increased viscosity and reduced water migration

ABSTRACT: The structural disorganization of different starches in a 1-ethyl-3-methylimidazolium acetate ([Emim][OAc])/water mixture (1:6 mol./mol.) at room temperature (25 °C) was studied. For normal cereal starches, which have pinholes randomly dispersed on the granule surface or only in the outermost annular region (wheat starch), the aqueous ionic liquid (IL) completely destroyed the granule structure within 1–1.5 h. Pea starch (PeS) granules with cracks were destroyed by the aqueous IL within 6 h. High-amylose maize starch (HAMS), as well as potato and purple yam starches (PoS and PYS), which have a dense and thick outer granule layer, were even more resistant to the action of the solvent. Structural disorganization was accompanied by increased viscosity and controlled the binding of water molecules with starch chains. From this study, we concluded that the surface characteristics of starch granule are an important factor affecting starch structural disorganization in an aqueous IL.

Keywords: Different starch cultivars; Aqueous ionic liquid; Starch dissolution; Starch granule destruction; Granule structure; Crystalline structure.

1 Introduction

There has been huge interest in developing biodegradable polymeric materials based on natural biopolymers due to the desire for achieving sustainability and taking advantage of the unique properties of these natural biopolymers (Seoud, Koschella, Fidale, Dorn, & Heinze, 2007). Starch is an abundant biopolymer widely used in both food and non-food applications due to its desirable properties such as low cost, biocompatibility, renewability, and biodegradability (Pérez & Bertoft, 2010). The shape (sphere, lobular, polyhedron, disk, or irregular tube) and size (the length of the long axis ranging from 0.5 to 100 μm) of starch granules vary largely with botanical source (Jane, et al., 1994; Wang & Copeland, 2015). Based on the X-ray diffraction (XRD) patterns, starches can be divided into A-, B- and C-types, which have different physicochemical properties (Lopez-Rubio, Flanagan, Gilbert, & Gidley, 2008; Wang, Yu, & Yu, 2008). C-type starches (for example Chinese yam starch) are shown to have both A- and B-type crystalline polymorphs, with the B-type polymorph in the center surrounded by the A-type polymorph (Wang, et al., 2007; Wang, et al., 2008; Wang, Yu, Yu, Chen, & Pang, 2007). The A- and B-type crystallites are considered to have the same double-helical configuration, but the way of packing and the water content in the crystallites are different (Pérez, Baldwin, & Gallant, 2009). The periphery of starch granules is the first barrier against hydrolysis and chemical actions (Nierle, Baya, Kersting, & D. Meyer, 1990). For maize and millet starches, there are pores distributed randomly on the granule surface, often in clusters and to different degrees, leading to high susceptibility to attack by enzymes or chemical reagents (Fannon, Hauber, & BeMiller, 1992). Large granules of wheat starch have pores along the equatorial groove, while there are wrinkles on the pea starch surface. For starches without pores on the granule surface,

such as potato and yam starches, their surface is corroded much more evenly with the action of amylases or chemical reagents (Gallant, Derrien, Aurnaitre, Guilbot, & Massy, 1973).

Because of strong inter- and intramolecular hydrogen bonds in semi-crystalline starch granules (Mäki-Arvela, Anugwom, Virtanen, Sjöholm, & Mikkola, 2010), starch cannot be fully dissolved in water at temperatures below 120 °C (Jan & Carl, 2010). Hence, other solvents are usually used for starch dissolution, including alkaline solution (Han & Lim, 2004), dimethyl sulfoxide (DMSO) (Jackson & NE, 1991), zinc chloride (Lina, et al., 2016), molten imidazole (Jordan, Schmidt, Liebert, & Heinze, 2014), and *N*-methyl morpholine-*N*-oxide (NMMO) (Koganti, Mitchell, Ibbett, & Foster, 2011). However, these solvents have disadvantages such as the tendency to cause starch degradation, being inflammable and explosive. Ionic liquids (ILs), a liquid salt with a melting point below 100 °C, are considered as "green" solvents for starch and cellulose (Rogers & Seddon, 2003). ILs have some unique physicochemical characteristics such as non-flammability, low vapor pressure, chemical stability, and recyclability (Earle, et al., 2006; Seoud, et al., 2007). ILs composed of imidazole cations coupled with anions (e.g. halide or carboxylic acid) have strong hydrogen-bonding capacity, can destroy inter- and intramolecular hydrogen bonds in biopolymer molecular networks, and dissolve biopolymers with reduced energy consumption (Li, et al., 2011; Wilpiszewska & Spychaj, 2011). The appealing properties of ILs have attracted considerable interest as solvents for the processing of biopolymer (e.g. cellulose, starch, and lignin).

The dissolution behavior of starch (rate and degree of granule disintegration) in ILs-based solvents

are affected by several factors, but not limited to the solvent effects only (Zhao, et al., 2015). Firstly, the type and structure of cations and anions of ILs can highly affect starch dissolution. For example, ILs with alkyl imidazolium and [OAc^-] or [Cl^-] have proved to be most effective at dissolving polysaccharides including starch (Lappalainen, Kärkkäinen, & Lajunen, 2013; Tan & Macfarlane, 2010). The difference in size between anion and cation (Papanyan, Roth, Wittler, Reimann, & Ludwig, 2013), the alkyl chain length of cation (Khan, Taha, Ribeiro-Claro, Pinho, & Coutinho, 2014; Ren, et al., 2019), and the hydrogen-bonding capacity of anion (Ren, et al., 2019) all determine the dissolving capability of ILs. Secondly, ILs, when mixed water, could be more powerful for starch dissolution than pure ILs. Previous studies showed that 1-ethyl-3-methylimidazolium acetate ([Emim][OAc])/water mixtures have a critical ratio for the most efficient dissolution of starch (Zhang, et al., 2017). The [Emim][OAc]/water ratio influences viscosity, the interaction between water and IL ions, and the mobility of water molecules, which all impact starch dissolution (Liu & Budtova, 2013; Wang, et al., 2019). However, the dissolution mechanism of starch in aqueous ILs at room temperature is still under debate. Recently, Wang et al. found that the damage of potato starch structure was less severe than maize starch in [Emim][OAc])/water mixtures (irrespective of mass ratio, 2:8, 4:6, 5:5, 6:4, 8:2, or 10:0), which could be due to its distinct surface morphology (Wang, et al., 2019). Among six starches to be dissolved in 78 % NMMO, cereal starches (A-type) were found to dissolve more rapidly and completely compared with B- and C-type starches (Kogantia, Mitchell, MacNaughtan, Hill, & Foster, 2015).

To better understand the mechanism of starch dissolution in aqueous ILs, this work focuses on cereal

(millet, maize, wheat, waxy maize, and high-amylose maize), tuber (potato and yam) and bean (pea) starches, which are widely used in food and non-food applications. Meanwhile, a [Emim][OAc]/water (1:6 mol./mol.) mixture was used as it is proved to be the most effective at dissolving maize starch (Wang, et al., 2019; Zhang, et al., 2017). The changes in morphology, crystalline structure, and rheological properties of these eight starches during room-temperature treatment by aqueous IL were monitored, based on which the underlying mechanisms are discussed. By examining the relationship between starch architecture and dissolution behavior, our findings can improve our understanding of starch structures and provide insights into the processing and industrial application of starch-based materials.

2 Materials and methods

2.1 Materials

Waxy maize starch (WMS) and high-amylose maize starch (HAMS, Hylon VII) were kindly provided by National Starch Specialties Ltd (Shanghai, China). Normal maize starch (NMS), potato starch (PoS), and wheat starch (WS) were obtained from Sigma-Aldrich Chemical Company (St Louis, Missouri, USA). Pea starch (PeS) was purchased from Yuanye Bio-Technology Co., Ltd (Shanghai, China). Foxtail millet Jingu 16 was provided by Shanxi Qinzhouhuang Millet Group Co., Ltd (Changzhi, Shanxi, China). Purple yam was bought from a local market (Deqing, Guangdong, China). Millet and purple yam starches (MiS and PYS) were isolated from the foxtail millet grains and purple yam tubers according to Qi et al. (Qi, et al., 2019) and Wang et al. (Wang, et al., 2006), respectively. [Emim][OAc] (95% purity and ≤ 0.5% moisture content) was purchased from Nuowei

Chemical Technology Co., Ltd (Wuhu, Anhui, China).

2.2 Analysis of chemical composition and particle size distribution of starches

The moisture, protein and lipid contents of the isolated starches were determined according to AOAC Official Methods 925.10 (AOAC, 1925), 954.01 (AOAC, 1955), and 920.39 (AOAC, 1920), respectively. Amylose content was determined by the iodine-binding colorimetric method (Qi, et al., 2019). The phosphorous content was determined by inductively coupled plasma mass spectrometry (ICAPQ, Thermo Fisher Scientific, German). The particle size distribution of starch granules was measured using a Bettersize 2000B Intelligent Laser Particle Size Analyzer (Better size Instruments Ltd, China). For particle size measurement, starch was evenly dispersed in a sample cell filled with distilled water to attain an obscuration of 15–20%.

2.3 Sample preparation

The [Emim][OAc]/water (1:6 mol./mol.) mixture was pre-made based on the following equation:

$$n_{IL} = \frac{95\% \cdot m_{IL}}{M_{IL}} \quad (1)$$

$$n_{water} \frac{m_{water} + 5\% \cdot m_{IL}}{M_{water}} \quad (2)$$

where n_{IL} and n_{water} are the moles of the IL and water, respectively, and n_{IL}:n_{water} = 1:6; m_{IL} and m_{water} are the weights of the IL (95% purity) and water added, respectively; M_{IL} and M_{water} are the molar masses of the IL and water (170.21 g/mol and 18 g/mol), respectively.

Mixing [Emim][OAc] and water generates heat. After the aqueous IL prepared was cooled to room temperature, different starch suspensions (5 wt%), i.e. 0.5 g of starch (wet basis) mixed in 9.5 g of

the aqueous IL, were prepared and stirred magnetically (300 rpm) at room temperature (25 °C) for 0.5 h, 1 h, 1.5 h, 6 h, and 24 h, after which five volumes of absolute ethanol was added. The samples were centrifuged at 4500 g for 15 min. The precipitates were washed using ethanol and centrifuged for three more times to remove residual [Emim][OAc]. The obtained starches were dried in an oven at 30 °C overnight and ground to pass through a 100-mesh sieve.

2.4 Characterization of starch samples

2.4.1 Differential scanning calorimetry (DSC)

The thermal properties of starch samples were examined by a differential scanning calorimeter (200 F3, Netzsch, Germany) equipped with a thermal analysis data station. Starch samples (approximately 3 mg) were weighed accurately into 40 μL aluminum pans, where deionized water was added to obtain a starch/water ratio of 1:3 (w/w). The starch/water mixtures were left to stand overnight at room temperature before DSC measurement. The samples were heated from 20 °C to 135 °C at a heating rate of 10 °C/min and an empty aluminum pan was used as the reference. The onset temperatures (T_o), peak temperatures (T_p), conclusion temperatures (T_c), and melting enthalpy changes (ΔH) were calculated using Proteus analysis software.

2.4.2 X-ray diffraction (XRD)

The crystallinity of starch samples was analyzed using an X-ray diffractometer (D8 Advance, Bruker, Germany) operating at 40 kV and 40 mA. Starch samples were equilibrated over a saturated NaCl solution for 7 days before measurement. Starch powders were packed tightly in a round glass cell

and scanned from 5° to 35° (2θ) at a rate of 1 °/min and a step size of 0.02°. Relative crystallinity was calculated as the ratio of the crystalline area to the total area between 5° and 35° (2θ) using Eva software provided with the instrument.

2.4.3 Attenuated total reflectance-Fourier transform infrared spectroscopy (ATR-FTIR)

The ATR-FTIR spectra for native and treated starch samples were determined using a Thermo Scientific Nicolet IS50 FTIR spectrometer (Thermo Fisher Scientific, USA). Starch samples (150 mg) were pressed into round tablets before being scanned in the range of 4000-400 cm^{-1} at a resolution of 4 cm^{-1}, and with an accumulation of 32 scans. The spectrum of an empty cell against air was recorded as the background. The ratio of absorbances at 1047/1022 cm^{-1} was calculated using OMNIC 9.2 software to estimate the short-range molecular order of starch samples.

2.4.4 Laser confocal micro-Raman spectroscopy

A Renishaw Invia Raman microscope system (Renishaw, Gloucestershire, UK) equipped with a Leica microscope (Leica Biosystems, Wetzlar, Germany) was used to obtain the Laser confocal micro-Raman (LCM-Raman) spectra for starch samples in the range of 3500-100 cm^{-1} at a resolution of 7 cm^{-1}. A 785 nm green diode laser source was used. The full width at half maximum (FWHM) of the band at 480 cm^{-1}, which is usually used to characterize the short-range molecular order of starch, was obtained using WIRE 2.0 software (Wang, et al., 2019).

2.4.5 Scanning electron microscopy (SEM)

The morphology of starch samples was examined using a scanning electron microscope (SU1510, Hitachi, Japan). Starch powders were scattered on the conductive tape stuck on aluminum stubs and then sputter-coated with gold before imaging at an accelerating voltage of 2 kV.

2.4.6 Light microscopy

A light microscope (DM-400 M-LED, Leica, Germany) was used to observe the changes in granule birefringence under normal and polarized lights. During the treatment of starches (5 wt%) by the aqueous IL in glass vials, a drop of the starch/IL/water suspension was quickly taken out to a glass slide and covered with a coverslip for imaging.

2.4.7 Rheological measurement

The viscosity of starch/IL/water suspensions was measured at 25 °C on an MCR 302 rheometer (Anton Par GmbH, Austria). The measuring system had a cone-plate geometry with a 4° angle and a 50 mm diameter. Before testing, starches were mixed with the aqueous IL in glass vials, and then the suspensions were applied onto the platform rapidly at different treatment time points. The shear rate was fixed at 300 s^{-1} for 2 h for measurement. To prevent any changes in water content in the suspensions, silicone oil was placed around the edge of the measuring cell and the insulation cover of the rheometer was applied.

2.4.8 Low-field nuclear magnetic resonance (LF-NMR)

A 20 MHz NMI20-025 V-I NMR analyzer (Niumag Co., Ltd, Suzhou, China) was used to analyze hydrogen proton migration during treatment of starch with the aqueous IL. At different time points (0 h, 0.5 h, 1 h, 1.5 h, 6 h, and 24 h), 5 g of a starch/IL/water suspension (5 wt% starch in the aqueous IL) was placed in a 15 mm NMR glass tube and inserted into the NMR-probe. The T_2 transverse relaxation time of samples was measured by a Carr-Purcell-Meiboom-Gill (CPMG) pulse sequence at 32 °C with a τ-value of 300 μs between 90° and 180° pulses (Li, et al., 2020). Data from 8000 echoes were acquired based on 4 scan repetitions, and the repetition time between two successive scans was 7 s.

2.4.9 Statistical analysis

All analyses except for XRD were performed at least in triplicate, and the results are reported as mean values and standard deviations. Analysis of variance (ANOVA) followed by post-hoc Duncan's multiple range tests ($p < 0.05$) was conducted to determine the significant differences between mean values using SPSS 19.0 software (SPSS Inc. Chicago, IL, USA).

3 Results and discussion

3.1 Granule sizes and chemical compositions of starch samples

Table 1 lists the compositions (moisture, protein, lipid, amylose and phosphorous contents) of the different starches. HAMS had the highest amylose content (69.5%) and WMS the lowest (0.7%). The amylose contents of PoS and PYS were 34.4% and 34.9% respectively while those of the rest

starches were about 25%. The moisture, lipid and protein contents of eight starches were in the range of 7.5-12.6%, 0.1-0.6%, and 0.1-0.5%, respectively. Organophosphates were detected in all starches, with the greatest amount observed for potato starch mainly due to the presence of phosphate groups (Blennowa, Nielsen, Baunsgaard, Mikkelsen, & BEngelsen, 2002). The average granule size of the eight starches, as reflected by mean particle diameters ($D_{4,3}$), was ranked in the order PoS (56.3 μm) > PYS > PeS > WS > WMS > NMS > HAMS > MiS (10.3 μm).

Table 1. Chemical composition and volume-equivalent mean diameter ($D_{4,3}$) of the different starches.

Starches	Moisture content (%)	Protein content (%)	Lipid content (%)	Amylose content (%)	$D_{4,3}$ (μm)	Phosphorous content (μg/g)
MiS	12.1 ± 0.1^{b}	0.1 ± 0.0^{c}	0.5 ± 0.1^{a}	23.2 ± 1.1^{d}	10.3 ± 0.2^{f}	409.38
WMS	7.5 ± 0.1^{e}	0.3 ± 0.1^{b}	0.1 ± 0.3^{d}	0.7 ± 0.1^{e}	15.7 ± 0.3^{e}	42.38
NMS	10.1 ± 0.2^{c}	0.5 ± 0.2^{a}	0.2 ± 0.0^{c}	24.2 ± 2.5^{cd}	15.2 ± 0.2^{e}	132.68
WS	9.1 ± 0.1^{d}	0.2 ± 0.1^{ab}	0.2 ± 0.1^{c}	28.2 ± 0.9^{c}	22.5 ± 0.6^{d}	317.24
HAMS	12.4 ± 0.3^{ab}	0.1 ± 0.0^{c}	0.2 ± 0.1^{c}	69.5 ± 0.8^{a}	10.7 ± 0.1^{f}	194.24
PoS	12.6 ± 0.0^{a}	0.3 ± 0.0^{b}	0.1 ± 0.0^{d}	34.3 ± 1.7^{b}	56.3 ± 3.0^{a}	567.75
PeS	9.1 ± 0.1^{d}	0.2 ± 0.1^{ab}	0.3 ± 0.1^{ab}	24.9 ± 2.9^{cd}	35.9 ± 0.8^{c}	21.14
PYS	10.6 ± 0.2^{bc}	0.4 ± 0.2^{a}	0.6 ± 0.1^{a}	34.9 ± 1.6^{b}	44.8 ± 0.7^{b}	116.90

Values are represented as mean ± standard deviation; Data followed by the different lower-case superscript letters in the same column were significantly different ($p < 0.05$).

3.2 Crystalline structures of starch samples treated with aqueous [Emim][OAc]

Native MiS, WMS, NMS, and WS exhibited a typical A-type diffraction pattern with reflections at 15°, 17°, 18°, and 23° (2θ) (**Fig. 1A**). During treatment with the aqueous IL, the diffraction peaks for MiS, WMS, and MS gradually became weaker and almost disappeared within 1 h, while it took 1.5 h for WS to become mostly amorphous.

Fig. 1B shows that the XRD peaks for B-type starches (HAMS, PoS, and PYS) at 5.6°, 15°, 17°, 21.9°, and 23.7° (2θ) became weaker during treatment with the aqueous IL but the crystalline structure remained after treatment for 24 h. In contrast, PeS displayed a typical C-type XRD pattern with two major peaks at about 17° and 23° and small peaks at around 5.6° and 15° (2θ). The diffraction peaks weakened greatly and mostly disappeared within 6 h, which was indicative of a substantial disruption of crystalline structure. The changes in the diffraction peaks of starches during the treatment with the aqueous IL correspond to a reduction in relative crystallinity (**Table 4**). This indicates that the aqueous IL gradually disrupted the long-range crystalline structure in these starches.

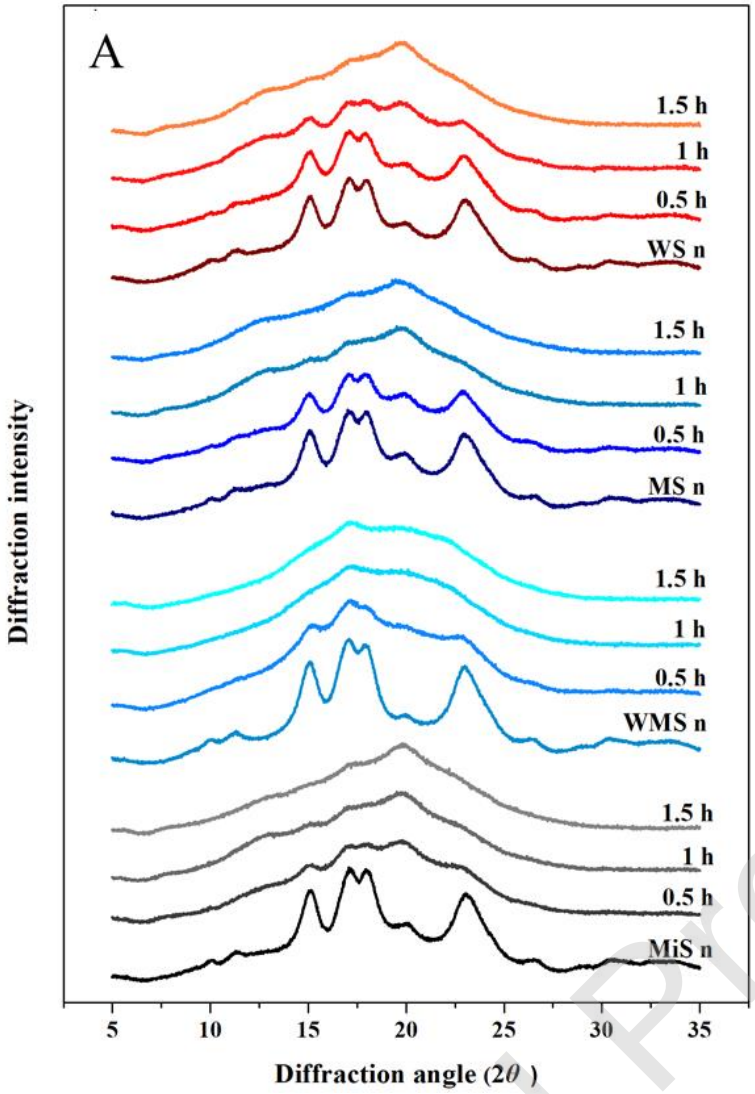

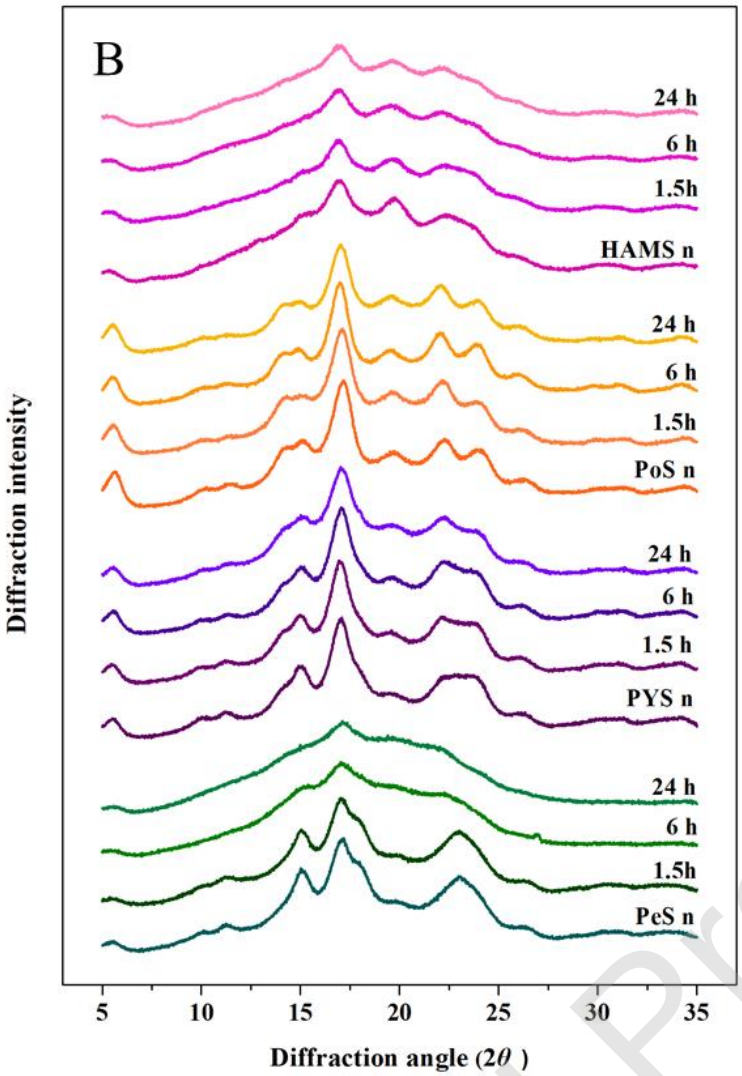

Figure 1 XRD patterns for the different starches treated with the [Emim][OAc]/water (1:6 mol./mol.) mixture: (A) MiS, WMS, NMS, and WS native (n) and treated for 0.5, 1, and 1.5 h; (B) HAMS, PoS, PYS, and PeS native (n) and treated for 1.5, 6, and 24 h.

3.3 Short-range molecular order of starch samples treated with aqueous [Emim][OAc]

The FTIR spectra for the different starch samples after treatment and the ratios of absorbances at 1047/1022 cm^{-1} ($R_{1047/1022}$) are shown in **Fig. S1** and **Table 2**, respectively. Meanwhile, the Raman spectra and the corresponding FWHM values of the band at 480 cm^{-1} for the different starch samples are presented in **Fig. S2** and **Table 3**, respectively. A higher $R_{1047/1022}$ value and a smaller FWHM value suggest a high degree of short-range molecular order in starch (Guo, Yu, Copeland, Wang, &

Wang, 2018; Wang, et al., 2018).

For all starches, $R_{1047/1022}$ decreased gradually with treatment time, although the decreases were not significant in some cases. For example, with treatment for 24 h, $R_{1047/1022}$ decreased from 0.72 to 0.64 for PoS, from 0.72 to 0.61 for HAMS, and from 0.76 to 0.65 for PYS with treatment for 24 h. Besides, FWHM for all the starches increased with treatment time. For example, with treatment for 1.5 h, FWHM increased from 15.18 to 17.24 for MiS, from 15.27 to 19.51 for WMS, from 15.54 to 17.59 for NMS, and from 15.53 to 18.31 for WS. The changes in $R_{1047/1022}$ and FWHM indicate that the short-range molecular order in the eight starches was disrupted increasingly with the duration of treatment by the aqueous IL.

Table 2. Ratios of absorbances at 1047/1022 cm^{-1} measured by FT-IR for the different starches treated with the [Emim][OAc]/water (1:6 mol./mol.) mixture for different duration.

Samples	IR ratio of absorbances at 1047/1022 cm^{-1}			
	Native	0.5 h	1 h	1.5 h
MiS	0.66 ± 0.05^{a}	0.62 ± 0.02^{ab}	0.60 ± 0.02^{b}	0.56 ± 0.01^{b}
NMS	0.68 ± 0.03^{a}	0.64 ± 0.03^{ab}	0.61 ± 0.02^{bc}	0.58 ± 0.05^{c}
WMS	0.69 ± 0.02^{a}	0.65 ± 0.01^{b}	0.64 ± 0.01^{b}	0.61 ± 0.01^{c}
WS	0.69 ± 0.02^{a}	0.63 ± 0.03^{b}	0.62 ± 0.02^{b}	0.60 ± 0.02^{b}
	Native	1.5 h	6 h	24 h
PoS	0.72 ± 0.04^{a}	0.70 ± 0.06^{ab}	0.69 ± 0.03^{ab}	0.64 ± 0.02^{b}
HAMS	0.72 ± 0.07^{a}	0.71 ± 0.03^{a}	0.66 ± 0.01^{ab}	0.61 ± 0.02^{b}
PeS	0.73 ± 0.02^{a}	0.68 ± 0.00^{b}	0.63 ± 0.02^{c}	0.62 ± 0.02^{c}
PYS	0.76 ± 0.05^{a}	0.73 ± 0.03^{ab}	0.70 ± 0.01^{b}	0.65 ± 0.01^{c}

Values are represented mean ± standard deviation; Data followed by the different lower-case superscript letters in the same row were significantly different ($p < 0.05$).

Table 3. Full width at half maximum (FWHM) values of the Raman band at 480 cm^{-1} for the different starches treated with the [Emim][OAc]/water (1:6 mol./mol.) mixture for different duration.

Samples	FWHM of 480 cm^{-1}			
	Native	0.5 h	1 h	1.5 h
MiS	15.18 ± 0.09^{a}	16.3 ± 0.23^{b}	17.21 ± 0.54^{c}	17.24 ± 0.59^{c}
NMS	15.54 ± 0.12^{a}	16.75 ± 0.25^{b}	17.39 ± 0.19^{c}	17.59 ± 0.17^{c}
WMS	15.27 ± 0.27^{a}	17.98 ± 0.06^{b}	18.29 ± 0.21^{b}	19.51 ± 0.27^{c}
WS	15.53 ± 0.10^{a}	16.27 ± 0.32^{b}	17.63 ± 0.12^{c}	18.31 ± 0.28^{d}
	Native	1.5 h	6 h	24 h
PoS	15.46 ± 0.28^{a}	15.90 ± 0.24^{b}	16.46 ± 0.08^{c}	18.56 ± 1.10^{d}
HAMS	14.66 ± 0.21^{a}	15.28 ± 0.53^{a}	16.12 ± 0.57^{b}	16.47 ± 0.27^{b}
PeS	15.18 ± 0.21^{a}	15.69 ± 0.15^{b}	18.18 ± 0.14^{c}	19.33 ± 0.24^{c}
PYS	15.1 ± 0.48^{a}	15.5 ± 0.31^{a}	16.36 ± 0.12^{b}	18.59 ± 0.04^{c}

Values are represented as mean ± standard deviation; Data followed by the different lower-case superscript letters in the same row are significantly different ($p < 0.05$).

3.4 Thermal properties of starch samples treated with aqueous [Emim][OAc]

Fig. 2 shows the DSC curves for the eight starches treated by the aqueous IL for different times and the corresponding thermal transition parameters (T_o, T_p, T_c, and ΔH) are listed in **Table 4**. A typical DSC endothermic transition was observed for all the native starches. After 1 h of treatment with the aqueous IL, the thermal transitions of MiS, WMS and NMS were not detected, but WS still presented a thermal transition. Hence, only the ΔH value for WS was determined (3.5 J/g) after 1 h of treatment. When the treatment time was 1.5 h, there was no gelatinization endotherm for the four A-type starches (MiS, WMS, NMS, and WS), indicating complete disruption of crystalline order in the starch granules. The lower thermal transition observed for MiS, WMS, and NMS after 1 h and 1.5 h of treatment and for WS after 1.5 h of treatment was attributed to starch retrogradation.

The peak temperatures (T_p) gradually shifted to higher temperatures during 1 h of treatment with the aqueous IL, indicating that the treatment preferentially disrupted less stable starch crystallites, leaving more stable crystallites to melt at a higher temperature (Wang, Wang, Guo, Liu, & Wang, 2017; Wang, Zhang, Wang, & Copeland, 2016).

Compared with the A-type starches, HAMS, PoS, PYS, and PeS had a smaller decrease in ΔH after the initial 1.5 h of treatment. Longer treatment resulted in a further substantial decrease in ΔH. For example, the ΔH value for PoS decreased from 17.3 J/g to 13.9 J/g for the first 1.5 h; longer treatment further reduced ΔH to 11.8 J/g at 6 h and 9.5 J/g at 24 h. The ΔH results here are in agreement with XRD results. For HAMS, PoS, PYS, and PeS, there was generally a decrease in T_p with prolonged treatment. The general trend of decreasing T_p for HAMS, PoS, PYS, and PeS suggests that the aqueous IL preferentially destructed more stable crystallites, hence the disruption of the crystalline structure was slow.

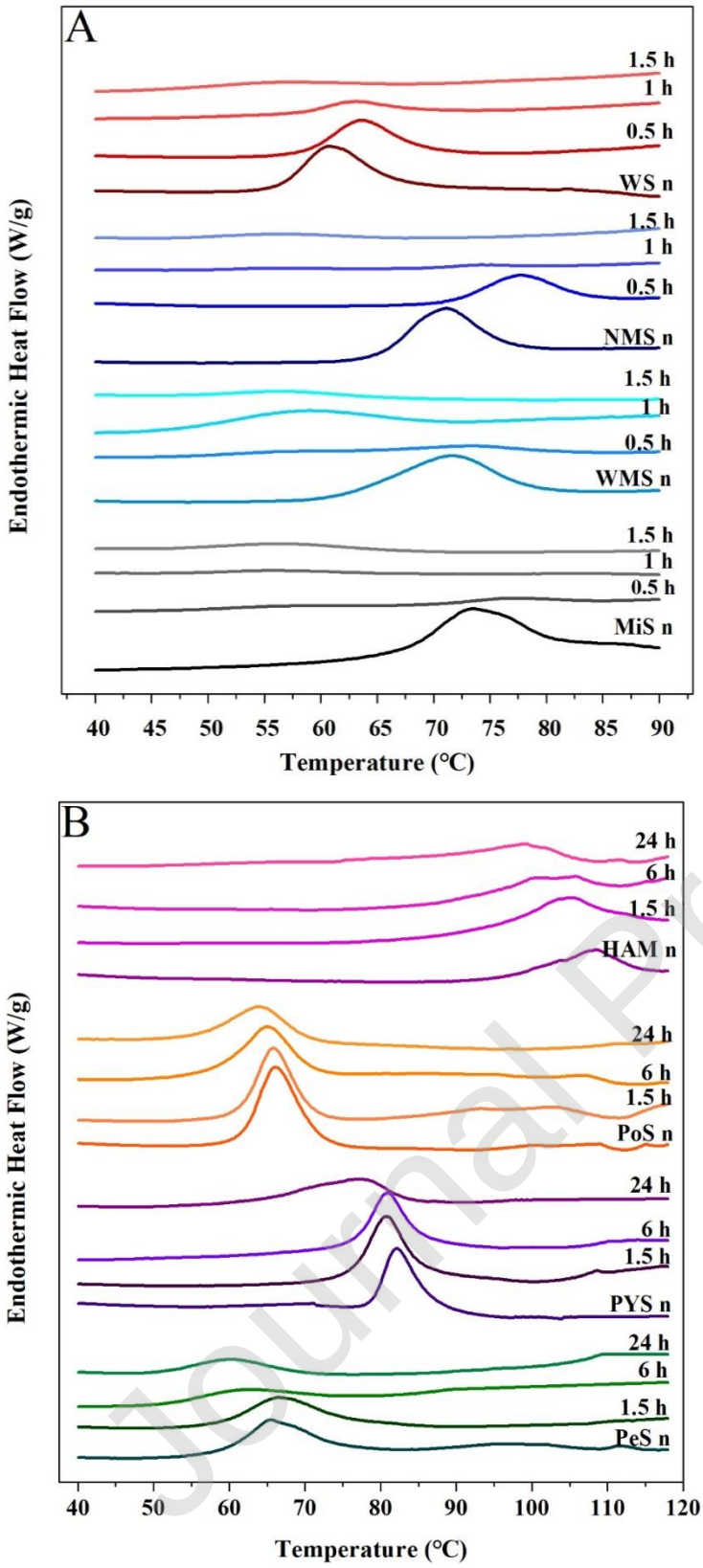

Figure 2 DSC curves for the different starches treated with the [Emim][OAc]/water (1:6 mol./mol.) mixture: (A) MiS, WMS, NMS, and WS native (n) and treated for 0.5, 1, and 1.5 h; (B) HAMS, PoS, PYS, and PeS native (n) and treated for 1.5, 6, and 24 h.

Table 4. Thermal properties and relative crystallinity of the different starches treated with the [Emim][OAc]/water (1:6 mol./mol.) mixture for different duration.

Samples	T_o (°C)	T_p (°C)	T_c (°C)	ΔH (J/g)	Relative crystallinity (%)
MiS					
Native	67.2 ± 0.2^{b}	73.3 ± 0.2^{b}	81.0 ± 0.8^{b}	14.3 ± 1.3^{b}	35.8 ± 1.2
0.5 h	70.1 ± 0.1^{b}	76.7 ± 0.4^{b}	82.9 ± 0.5^{b}	1.4 ± 0.1^{a}	8.9 ± 1.6
1.0 h	51.5 ± 0.5^{a}	55.3 ± 1.7^{a}	63.6 ±3.8^{a}	0.6 ±0.3^{a}	ND
1.5 h	51.0 ± 1.1^{a}	56.0 ± 0.2^{a}	65.7 ± 1.5^{a}	1.7 ± 0.1^{a}	ND
WMS					
Native	62.1 ± 0.5^{b}	71.7 ± 0.2^{b}	78.4 ± 0.4^{c}	13.7 ± 0.8^{c}	49.0 ± 2.5
0.5 h	65.2 ± 1.7^{c}	73.2 ± 1.3^{b}	80.5 ± 1.0^{c}	1.6 ± 0.3^{a}	11.1 ± 3.6
1.0 h	49.0 ± 0.7^{a}	58.8 ± 0.5^{a}	68.7 ± 0.8^{b}	5.2 ±1.7^{b}	ND
1.5 h	47.4 ± 1.3^{a}	57.1 ± 0.3^{a}	62.8 ± 2.2^{a}	1.6 ± 0.4^{a}	ND
NMS					
Native	65.1 ± 0.3^{b}	71.0 ± 0.14^{b}	76.6 ± 0.2^{b}	12.2 ± 1.2^{a}	30.0 ± 2.0
0.5 h	66.4 ± 0.2^{c}	72.7 ± 0.3^{c}	79.1 ± 0.6^{c}	6.9 ± 0.7^{b}	18.3 ± 2.1
1.0 h	67.6 ± 0.2^{d}	73.5 ± 1.0^{c}	82.7 ± 0.4^{d}	0.4 ± 0.1^{c}	ND
1.5 h	51.3 ± 0.5^{a}	56.1 ± 1.1^{a}	63.0 ± 2.6^{a}	1.3 ± 0.2^{c}	ND
WS					
Native	56.3 ± 0.1^{b}	60.8 ± 0.1^{b}	67.1 ± 0.3^{b}	10.1 ± 0.5^{d}	32.5 ± 0.8^{a}
0.5 h	58.7 ± 0.3^{c}	63.8 ± 0.1^{b}	69.2 ± 0.3^{b}	7.3 ± 1.3^{c}	22.1 ± 2.0^{b}
1.0 h	58.2 ± 0.1^{c}	63.3 ± 0.2^{b}	69.1 ± 0.1^{b}	3.5 ± 0.3^{b}	6.7 ± 0.4^{c}
1.5 h	49.7 ± 2.3^{a}	54.2 ± 3.9^{a}	60.0 ± 4.1^{a}	0.6 ± 0.8^{a}	ND
HAMS					
Native	100.2 ± 0.2^{a}	108.0 ± 1^{a}	115.1 ± 1.3^{a}	8.0 ± 0.5^{a}	21.0 ± 1.36^{a}
1.5 h	97.3 ± 1.7^{a}	102.5 ± 3.5^{ab}	109.6 ± 0.7^{ab}	6.0 ± 0.6^{b}	13.7 ± 1.2^{b}
6 h	96.7 ± 0.4^{ab}	100.0 ± 0.0^{b}	107.4 ± 2.3^{ab}	3.8 ± 0.6^{c}	11.5 ± 0.8^{b}
24 h	93.5 ± 1.8^{b}	97.1 ± 2.8^{b}	103.5 ± 4.7^{b}	3.0 ± 0.1^{c}	10.3 ± 0.9^{b}
PoS					
Native	61.8 ± 0.1^{a}	66.1 ± 0.1^{a}	72.0 ± 0.2^{a}	17.3 ± 0.5^{a}	39.1 ± 1.2^{a}
1.5 h	61.7 ± 0.1^{a}	66.0 ± 0.2^{a}	71.4 ± 0.2^{ab}	13.9 ± 0.6^{b}	35.0 ± 1.1^{b}
6 h	59.1 ± 0.2^{b}	65.1 ± 0.1^{b}	71.2 ± 0.5^{b}	11.8 ± 0.3^{c}	26.5 ± 3.9^{c}
24 h	53.9 ± 0.3^{c}	61.1 ± 0.1^{c}	68.6 ± 0.4^{c}	9.5 ± 0.4^{d}	21.0 ± 2.3^{d}
PYS					
Native	78.9 ± 0.0^{a}	82.1 ± 0.1^{a}	86.9 ± 0.2^{a}	12.4 ± 0.5^{a}	40.0 ± 2.5^{a}
1.5 h	76.9 ± 0.1^{b}	80.7 ± 0.1^{b}	85.2 ± 0.1^{b}	12.0 ± 0.4^{b}	33.6 ± 1.0^{b}
6 h	76.9 ± 0.1^{b}	81.0 ± 0.1^{b}	85.7 ± 0.5^{b}	11.4 ± 0.3^{b}	31.0 ± 0.9^{b}
24 h	65.7 ± 0.2^{c}	76.5 ± 0.9^{c}	83.4 ± 0.2^{c}	6.9 ± 0.6^{c}	25.4 ± 0.7^{c}
PeS					
Native	60.5 ± 1.0^{a}	65.8 ± 0.3^{a}	73.1 ± 1.9^{a}	11.5 ± 0.5^{a}	35.2 ± 2.5^{a}
1.5 h	59.4 ± 0.2^{a}	66.6 ± 0.1^{b}	74.5 ± 0.6^{b}	9.2 ± 0.2^{b}	29.6 ± 1.4^{b}
6 h	52.1 ± 0.8^{b}	62.0 ± 0.3^{c}	71.0 ± 0.7^{c}	5.2 ± 0.1^{c}	10.1 ± 4.1^{c}
24 h	51.6 ± 0.3^{b}	59.9 ± 0.7^{d}	68.2 ± 0.8^{d}	4.8 ± 0.1^{c}	3.6 ± 0.8^{d}

Values are represented as mean ± standard deviation; Data followed by the different lower-case superscript letters in the same column were significantly different ($p < 0.05$); ND, not determined.

3.5 Granule morphology of starch samples treated with aqueous [Emim][OAc]

The effect of the aqueous IL on starch granule morphology at room temperature was observed under light microscopy and SEM (**Fig. 3)**. MiS, WMS, and NMS all had a small granule size, angular or irregular shapes, and a rough surface containing many randomly distributed indentations with pores in the center of indentation. Upon treatment of these three starches by the aqueous IL, the pores on the surface became larger and cracks were formed at 0.5 h and 1 h. The granules sagged inward until finally, the granules were broken completely at 1.5 h, exposing the internal cavity. Among these three starches, WMS was the most susceptible to treatment, for example, the granules lost its morphology completely and agglomerated into more dense lumps after 1 h of treatment. Under polarized light, the birefringent patterns (Maltese crosses) of WMS and MiS almost disappeared at 0.5 h, while at 1 h for NMS.

SEM images show that WS is composed of big discoid-like granules (A-type) and small spherical granules (B-type). The granule surface was mostly smooth and the pinholes could only be found at the equatorial circular depression of the discoid granules. At 0.5 h, the outermost annular region near the equatorial trough was most sensitive to solvent corrosion and the peeling of the granules occurred. With prolonged treatment, this tangential degradation led to the cutting of the outermost annular region and further inwards tangential destruction until the stable central nucleus was exposed. By 1.5 h, the central nucleus was completely destroyed. Light microscopy images also show that the

outermost annular region was destroyed first and the birefringent patterns in the granule center remained until 0.5 h; afterwards, the birefringent pattern gradually became smaller and disappeared after 1.5 h of treatment.

The morphological changes of MiS, WMS, NMS, and WS indicate that starch granules with randomly distributed pinholes on their surface dissolved faster than those with pinholes concentrated at the outermost annular region while other places were smooth. More specifically, the distribution of pinholes could determine how the aqueous IL penetrates into the granule, whether radially or tangentially.

PeS granules are mostly ellipsoids with wrinkles on their surface, which deepened and cracked after 1.5 h of treatment by the aqueous IL. The outermost annular layer was separated from the center after 6 h of treatment. At 24 h, the outermost layer of starch granules peeled off, accompanied by the fading of the birefringent patterns. SEM images show that PoS and PYS have spherical granules and a smooth surface. During the aqueous IL treatment, many small cracks developed on the outer layers of PoS and PYS, and joined together to form large cracks eventually, leading to complete disintegration of some granules after 24 h of treatment. Birefringent patterns on the granules were observed to become increasingly blurred mainly during 6-12 h and almost disappeared at 24 h. HAMS granules are small in size and have irregular shapes with a smooth surface. The aqueous IL treatment also caused corrosion of HMAS granules but without significant cracking or rifting. It is proposed that the absence of pores on the granules of PeS, HAMS, PoS, and PYS, especially the

thick and compact outer layers of PoS and PYS, make it difficult for the aqueous IL to destroy the granule structures.

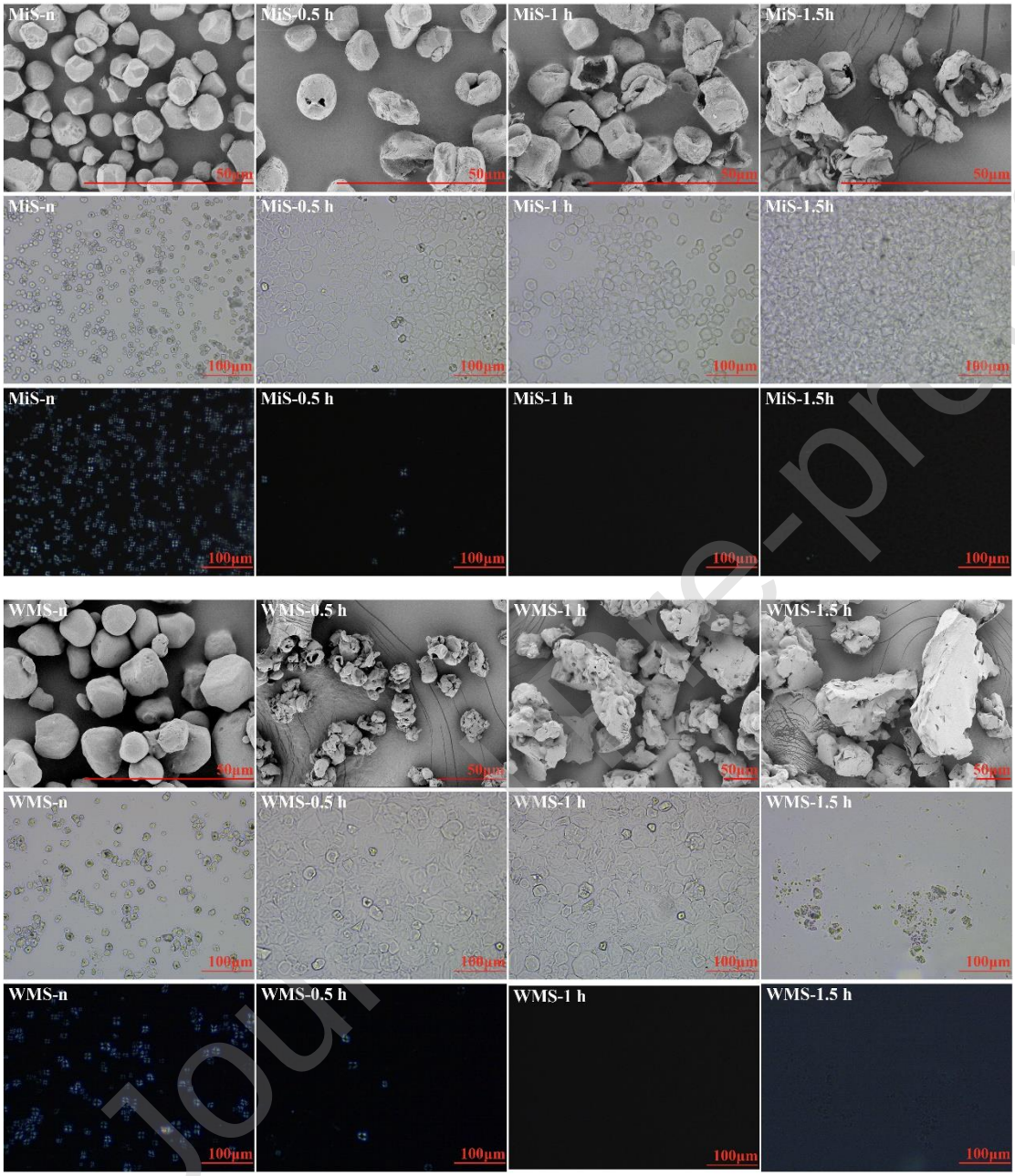

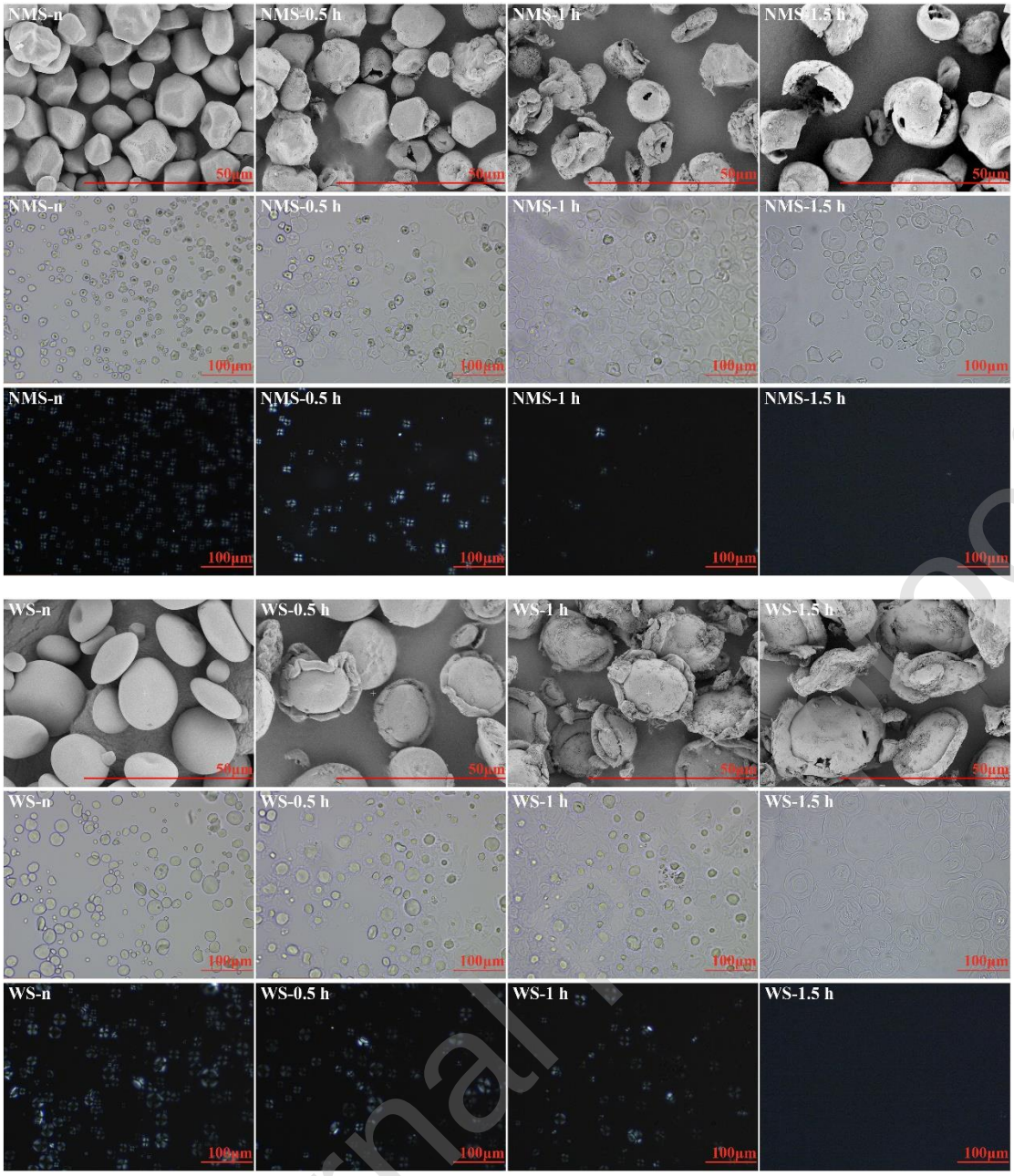

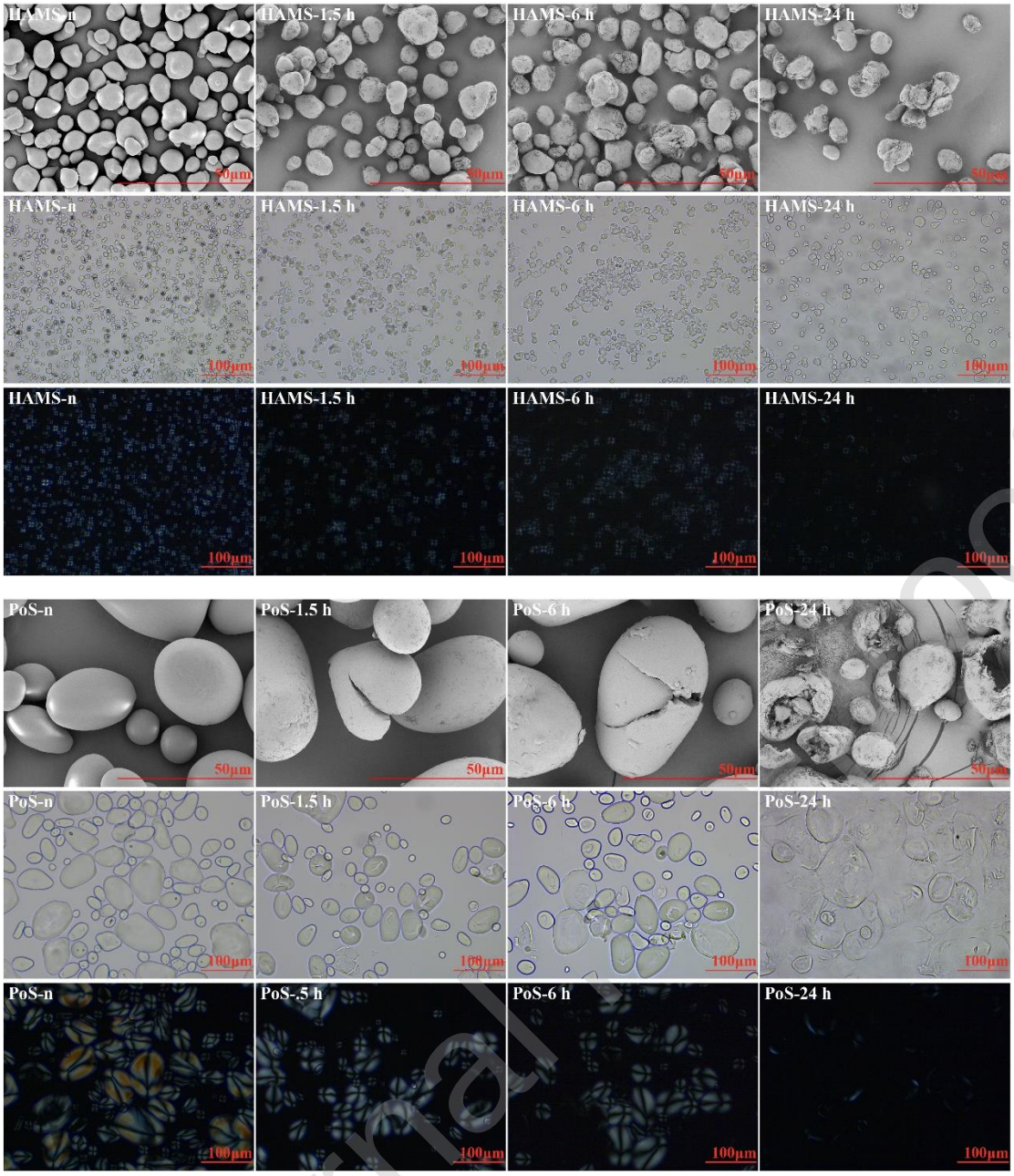

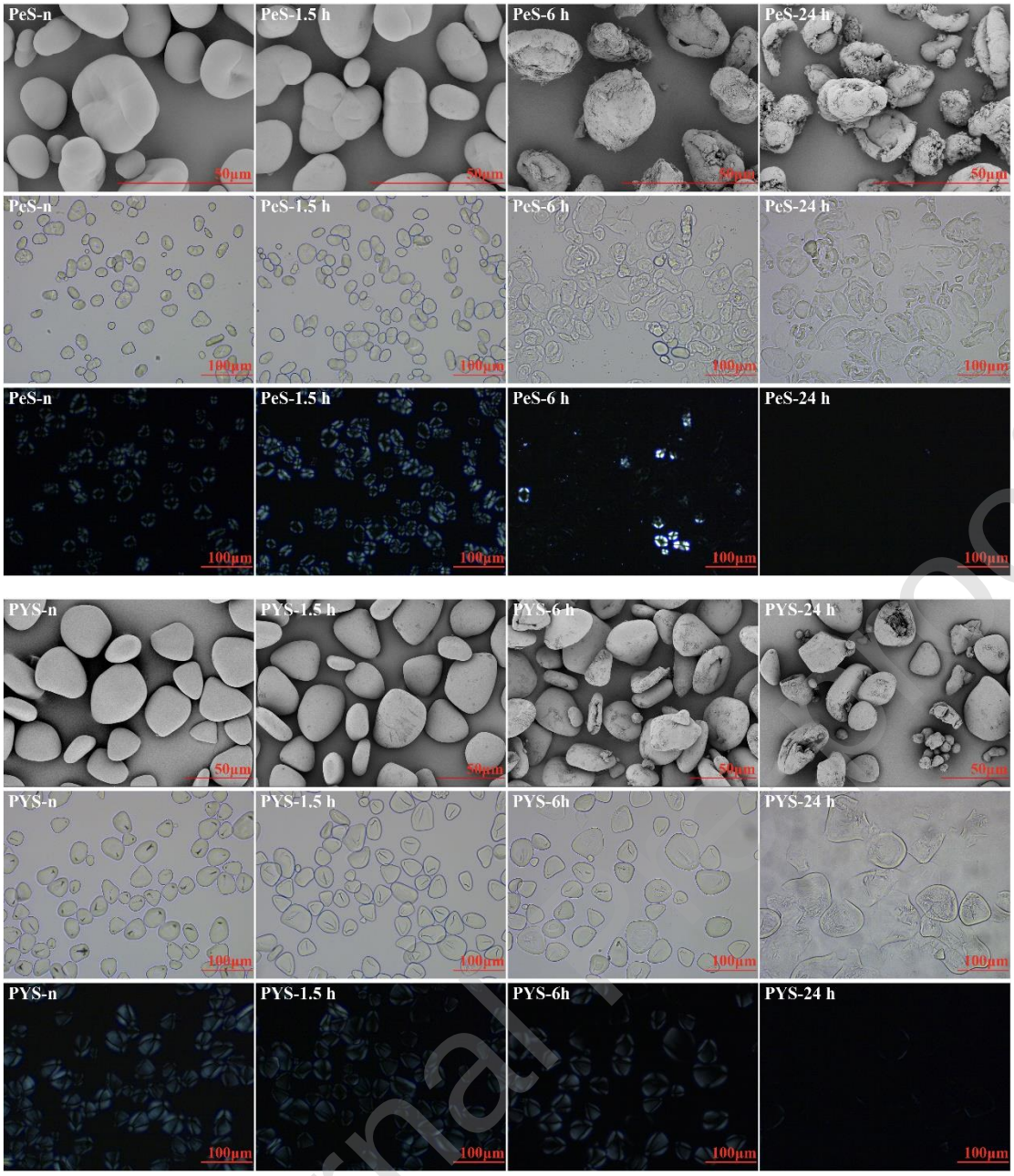

Figure 3 Representative SEM (Line 1) and light microscopy images under normal (Line 2) and polarized light (Line 3) of MiS, WMS, NMS, WS, HAMS, PoS, PYS, and PeS native and treated with the [Emim][OAc]/water (1:6 mol./mol.) mixture for different duration.

3.6 Rheological properties of starch samples in aqueous [Emim][OAc]

The viscosity of the IL/water (1:6 mol./mol.) mixture at a constant shear rate (300 s^{-1}) and

temperature (25°C) was around 12 mPa·s, which remained essentially unchanged during the shearing process (Wang, et al., 2019). The viscosity of starch (5 wt%) in the same aqueous IL as a function of treatment time was monitored (**Fig. 4**). During the first 2 h (**Fig. 4A**), the viscosity of the WMS/IL/water suspension rose rapidly from 14.5 mPa·s to 685.9 mPa·s at around 0.5 h of treatment, followed by a slow increase up to 1184.8 mPa·s at 2 h. Similar viscosity changes were also observed for MiS, NMS, and WS, although the increase occurred at a different rate and to a different degree. The changes indicate that the granule structure was disrupted gradually during treatment, leading to the dissolution of starch and increased viscosity of the solutions. In contrast, there were no apparent changes for the suspensions of HAMS, PoS, PYS, and PeS over 2 h of treatment, meaning that the starch structure was not disrupted in the aqueous IL/water within the first 2 h (Zhang, et al., 2017). For HAMS, PoS, PYS, and PeS, the viscosity only marginally increased during 6–8 h (in particular, for HAMS, from 17.7 mPa·s to 27.3 mPa·s) (**Fig. 4B**). Prolonged treatment increased further the viscosity of these starch suspensions, with PeS presenting the highest viscosity of 475.38 mPa·s at 26 h. These changes in viscosity for HAMS, PoS, PYS and PeS indicate that the dissolution of these starches occurred slowly but progressively during the whole treatment.

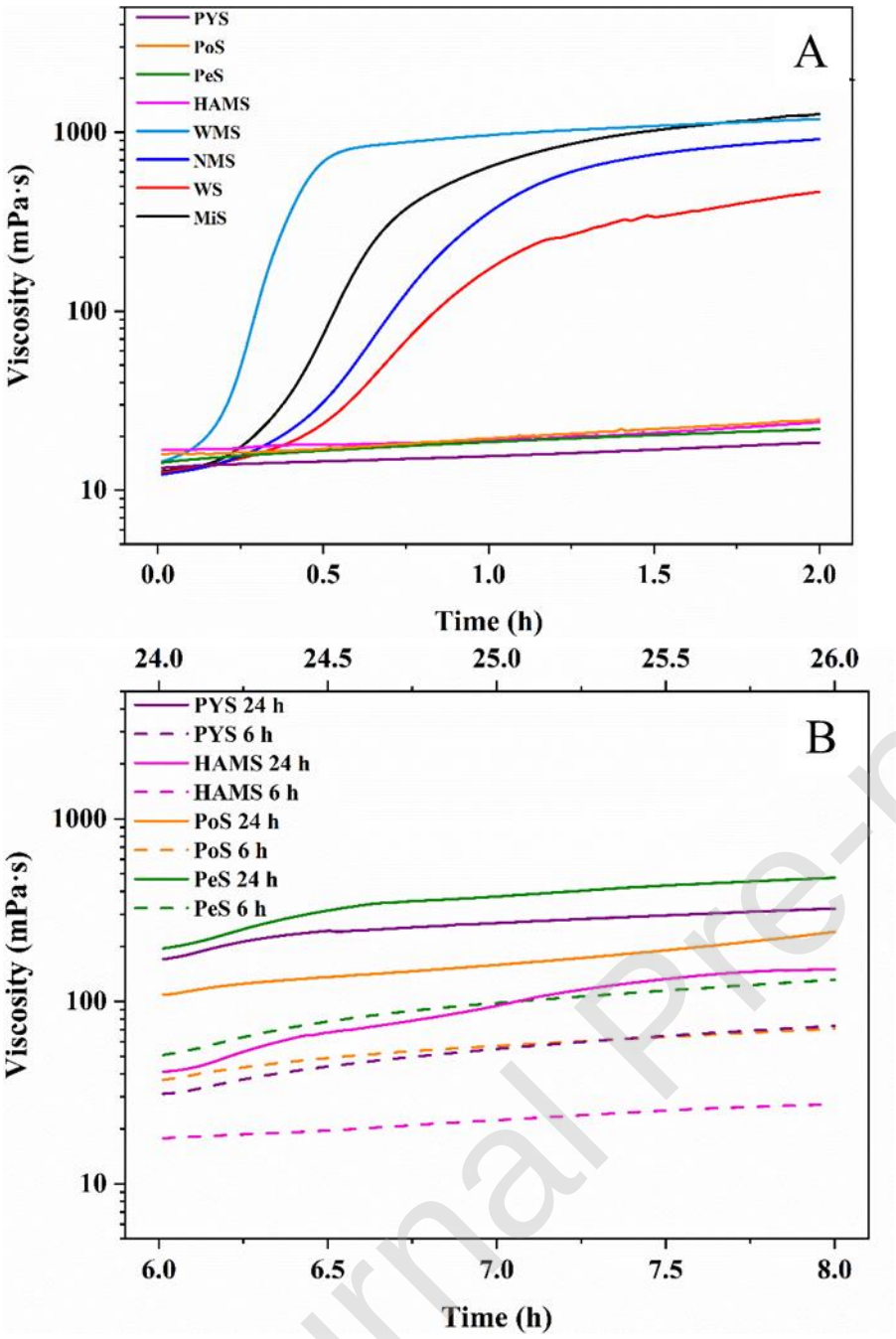

Figure 4 Viscosity profiles of the different starches treated with the [Emim][OAc]/water (1:6 mol./mol.) mixture: (A) MiS, WMS, NMS, WS, HAMS, PoS, PYS, and PeS during 0-2 h of treatment; (B) HAMS, PoS, PYS, and PeS during 6-8 h and 24-26 h of treatment.

3.7 T_2 distribution of aqueous [Emim][OAc] and starch samples treated with aqueous [Emim][OAc]

The state and distribution of water in different systems can be characterized by low field-NMR, with a longer T_2 relaxation time reflecting a higher degree of molecular mobility (Li, et al., 2020). From the results of the LF-NMR measurement (**Fig. 5**), there were three different proton groups from the relaxation signals, which can be ascribed to strongly bound water (0.01-1 ms), weakly bound water (1-100 ms), and free water (100-10000 ms) (Li, et al., 2015; Tang H, 2001). At room temperature, there were small changes in the T_2 relaxation time of proton groups over time (**Fig. 5a** and **f**), suggesting the water in the IL/water mixture is relatively stable. However, the proportion of free water in starch/IL/water suspensions declined. For MiS, WMS, NMS, and WS, the relaxation time of free water in the suspensions decreased along with reduced amplitude (peak height). For example, the T_2 relaxation time for the WMS/IL/water suspension changed from 1431.5-4994.5 ms to 47.6-943.7 ms) after 0.5 h. The T_2 relaxation time curve was stable for WMS and MiS suspensions within 0.5 h whereas for NMS and WS suspensions, within at least 1 h. For WMS, MiS, and NMS suspensions (**Fig. 5a-d**), the relaxation time peak between 50-2000 ms changed from a narrow singlet into a doublet, indicating a decrease in the mobility of water molecules due to the formation of weakly bound water. For HAMS and PeS, the T_2 relaxation time of free water changed significantly at 1.5 h or 6 h, respectively, whereas, for PYS and PeS, the change was minor up to 24 h. The results indicated that the mobility of water molecules in these starch suspensions was changed to a much smaller degree compared with other starch suspensions, consistent with the starch structural changes caused by the aqueous IL.

A

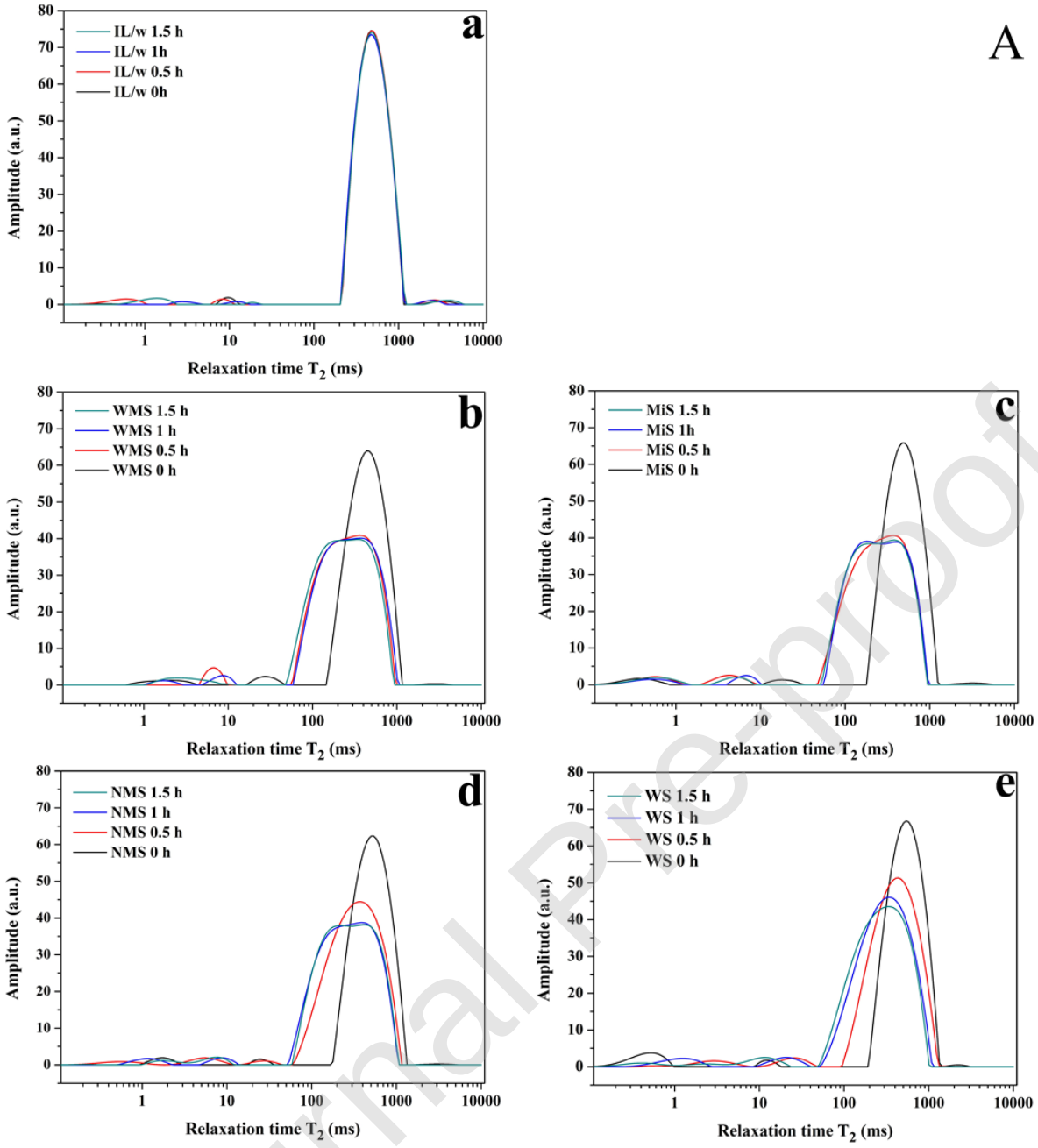

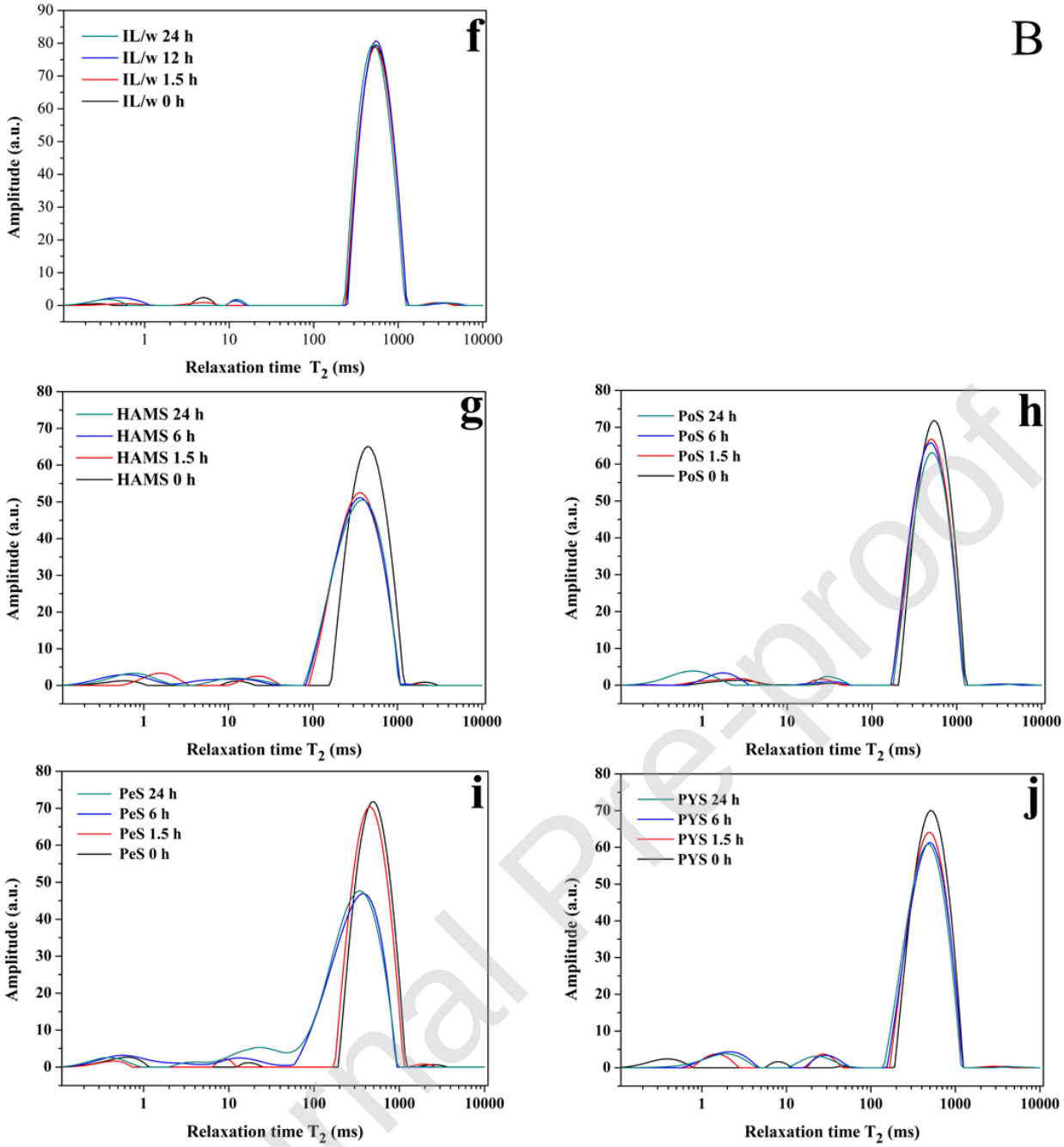

Figure 5 Carr-Purcell-Meiboom-Gill (CPMG) proton distributions of water molecules in the [Emim][OAc]/water (1:6 mol./mol.) mixture during treatment of the different starches: (a) and (f) the [Emim][OAc]/water mixture at 0, 0.5, 1, 1.5, 6, and 24 h; (b), (c), (d), and (e) WMS, MiS, NMS, and WS at 0, 0.5, 1, and 1.5 h; (g), (h), (i), and (j) HAMS, PoS, PYS, and PeS at 0, 1.5, 6, and 24 h.

3.8 Further discussion

In this study, the dissolution behavior of the eight starches in aqueous [Emim][OAc] was investigated by characterizing the structural changes of starch and the viscosity of starch suspensions during treatment. The results showed that the surface structure of starch granules is key to affecting the dissolution behavior of starch in an aqueous IL. Two different patterns for starch dissolution are proposed based on the results of granule morphology and thermal transition (**Fig. 6**). For MiS, WMS, NMS, and WS, the pinholes on the surface could allow the IL/water to penetrate into the granule easily, resulting in endo-corrosion of starch granules. As shown in **Fig. 6A(a)**, MiS, WMS, and NMS, which have holes randomly distributed on the surface, only needed 1 h for the full destruction of the granules, while it took a longer time (1.5 h) for WS, which has holes concentrated in the outermost annular region while having other surface areas being smooth, to be fully destroyed as illustrated in **Fig. 6A(b)**.

For MiS, WMS, NMS, and WS, less stable crystallites of the starch granule were first destroyed, followed by more stable structures, resulting in the endothermic transition shifting to a higher temperature. Further treatment would destroy all the helical structures and crystallites in starch as shown by DSC and XRD results. With the effective destruction of the starch granule structure, amylose was liberated from the granule, which significantly increased the viscosity of the solution and hindered the mobility of water molecules (Zhang, et al., 2017).

Starch granules (PoS, PYS, and PeS) with a relatively smooth surface and a thick outer layer are

more resistant to the attack by the aqueous IL. In this case, the corrosion of starch granules by the solvent started from the surface, leading to the formation of cracks (see **Fig. 6B** and SEM images). As the action of the solvent occurred firstly on the stable surface structures, the endothermic transition occurred at a lower temperature and the destruction process was slow. These starches still showed an endothermic peak and crystallinity after 24 h of treatment. In particular, for large starch granules such as potato starch granules, this exo-corrosion from the surface could not reach the entire starch granule within 24 h, leaving some starch crystallites intact. Therefore, the mobility of water molecules was hindered and the change in viscosity due to the leaching of amylose chains was small.

For maize starches, amylose content has an impact on the destruction process with the aqueous IL as shown by microscopy, DSC and XRD results. HAMS were more rigid and resistant to the solvent than NMS and WMS. The different rate and extents of granule destruction for WMS, NMS, and HAMS with the aqueous IL confirm that starch with a higher amylose content is more stable in the aqueous IL with less fragmentation of the granule.

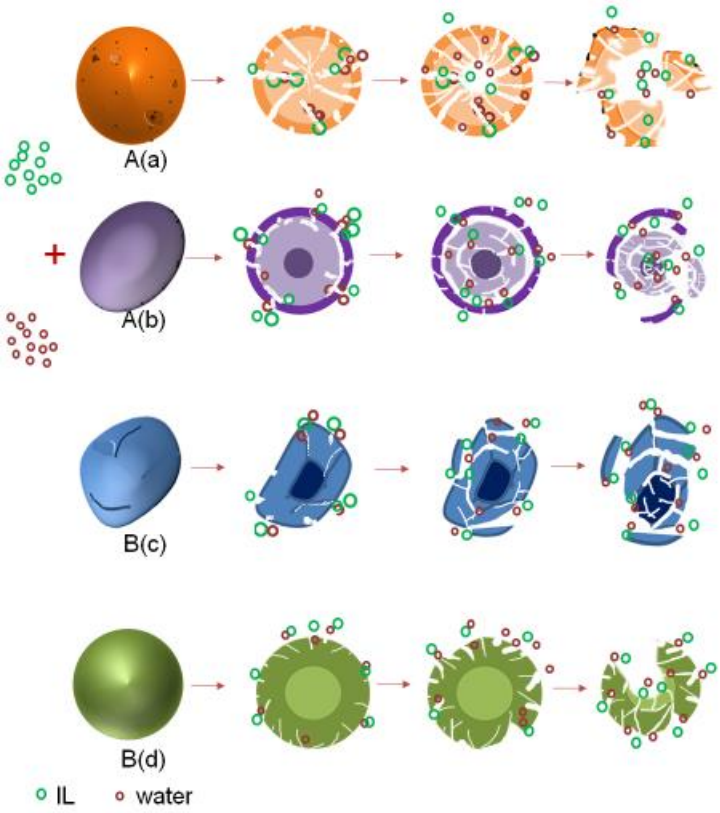

Figure 6 Schematic representation of starch disorganization as affected by aqueous ionic liquid: (A) endo-corrosion pattern for (a) WMS, MiS, NMS, and (b) WS; (B) exo-corrosion pattern for (c) PeS, (d) HAMS, PoS, and PYS.

4 Conclusions

While the [Emim][OAc]/water (1:6 mol./mol.) mixture can effectively destruct the starch multiscale structure at room temperature 25 °C, the way and degree of damage were different for starches with different starch surface morphology. For starches with pores (MiS, WMS, NMS, and WS), the corrosion by the aqueous IL follows an inside-out pattern and the destruction to the granules is fast and even. In contrast, for starches with a relatively smooth surface (HAMS, PoS, PYS, and PeS), the corrosion can only start from the surface. After the aqueous IL treatment, WMS agglomerates into

dense lumps whereas, for the other starches, granule fragments are left. The suspension viscosity and the mobility of water molecules in the system are influenced by the dissolution process. Our results clearly indicate that the destruction process of starch by an aqueous IL is predominantly determined by granule surface structure, meanwhile being strongly impacted by amylose content. Our findings reveal the structural evolution of starch granules during aqueous IL treatment, which could provide an insight into the design of dissolution and modification processes for different starches.

Declaration of Competing Interest

There is no conflict of interests to declare.

Acknowledgement

The authors gratefully acknowledge the financial support from the National Natural Science Foundation of China (32030084 and 31871796), Natural Science Foundation of Tianjin Municipal Science and Technology Commission (20ZYJDJC00040 and 17JCJQJC45600).

References

AOAC. (1920). AOAC Official Method 920.39 Fat (Crude) or Ether Extract in Animal Feed *Washington, DC : Association of Official Analytical Chemists*.

AOAC. (1925). AOAC Official Method 925.10 Solids (Total) and Moisture in Flour *Washington, DC : Association of Official Analytical Chemists*.

AOAC. (1955). AOAC Official Method 954.01 Protein (Crude) in Animal Feed and Pet Food *Washington, DC : Association of Official Analytical Chemists*.

Blennowa A., Nielsen T. H., Baunsgaard L., Mikkelsen R., & BEngelsen S. (2002). Starch phosphorylation_ a new front line in starch research. *Trends in Plant Science, 7*(10), 445-450.

Earle M. J., Esperanc J. M. S. S., Gilea M. A., Lopes J. N. C., Rebelo L. s. P. N., Magee J. W., Seddon K. R., & Widegren J. A. (2006). The distillation and volatility of ionic liquids. *Nature, 439*(7078), 831-834.

Fannon J. E., Hauber R. J., & BeMiller J. N. (1992). Surface pores of starch granules[J]. *Cereal Chemistry, 69*(3), 284-288.

Gallant P. D., Derrien A., Aurnaitre A., Guilbot e. A., & Massy. (1973). Dégradation in vitro de l'amidon par le suc pancréatique. Etude par microscopie électronique à transmission et à balayage. *Starch - Stärke, 25*(2), 56-64.

Han J.-A., & Lim S.-T. (2004). Structural changes in corn starches during alkaline dissolution by vortexing. *Carbohydrate Polymers, 55*(2), 193-199.

Jackson D. S., & NE L. (1991). Solubility Behavior of Granular Corn Starches in Methyl Sulfoxide

(DMSO) as Measured by 1991 High Performance Size Exclusion Chromatography. *Starch-Stärke, 43*(11), 422-427.

Jan D., & Carl H. R. (2010). Principles of cereal science and technology authors provide insight into the current state of cereal processing. *Cereal Foods World, 55*(1), 21-22.

Jane J.-l., Kasemsuwan T., Leas S., IA A., Zobel H., IL D., Robyt J. F., & IA A. (1994). Anthology of Starch Granule Morphology by Scanning Electron Microscopy. *Starch - Stärke, 46*(4), 121-129.

Jordan T., Schmidt S., Liebert T., & Heinze T. (2014). Molten imidazole – a starch solvent. *Green Chemistry, 16*(4), 1967-1973.

Khan I., Taha M., Ribeiro-Claro P., Pinho S. o. P., & Coutinho J. o. A. P. (2014). Effect of the cation on the interactions between alkyl methyl imidazolium chloride ionic liquids and water. *Journal of Physical Chemistry B, 118*(35), 10503-10514.

Koganti N., Mitchell J. R., Ibbett R. N., & Foster T. J. (2011). Solvent effects on starch dissolution and gelatinization. *Biomacromolecules, 12*(8), 2888-2893.

Kogantia N., Mitchell J., MacNaughtan W., Hill S., & Foster T. (2015). Effect of granule organisation on the behaviour of starches in the NMMO (N-methyl morpholine N-oxide) solvent system. *Carbohydr Polymers, 116*, 103-110.

Lappalainen K., Kärkkäinen J., & Lajunen M. (2013). Dissolution and depolymerization of barley starch in selected ionic liquids. *Carbohydrate Polymers, 93*(1), 89-94.

Li P., Li Y., Wang L., Zhang H., Qi X., & Qian H. (2020). Study on water absorption kinetics of black beans during soaking. *Journal of Food Engineering, 283*.

Li T., Tu C., Rui X., Gao Y., Li W., Wang K., Xiao Y., & Dong M. (2015). Study of water dynamics in the soaking, steaming, and solid-state fermentation of glutinous rice by LF-NMR: a novel monitoring approach. *Journal of agricultural and food chemistry, 63*(12), 3261-3270.

Li W., Sun N., Stoner B., Jiang X., Lu X., & Rogers R. D. (2011). Rapid dissolution of lignocellulosic biomass in ionic liquids using temperatures above the glass transition of lignin. *Green Chemistry, 13*(8), 2038-2047.

Lina M., Shanga X., Liua P., Xie F., Chen X., Sun Y., & Wana J. (2016). Zinc chloride aqueous solution as a solvent for starch. *Carbohydr Polymers, 136*, 266-273.

Liu W., & Budtova T. (2013). Dissolution of unmodified waxy starch in ionic liquid and solution rheological properties. *Carbohydr Polymers, 93*(1), 199-206.

Lopez-Rubio A., Flanagan B. M., Gilbert E. P., & Gidley M. J. (2008). A novel approach for calculating starch crystallinity and its correlation with double helix content: a combined XRD and NMR study. *Biopolymers, 89*(9), 761-768.

Mäki-Arvela P., Anugwom I., Virtanen P., Sjöholm R., & Mikkola J. P. (2010). Dissolution of lignocellulosic materials and its constituents using ionic liquids—A review. *Industrial Crops and Products, 32*(3), 175-201.

Nierle W., Baya A. W. E., Kersting H. J., & D. Meyer D. (1990). Lipids and rheological properties of starch. Part II: The effect of granule surface material on viscosity of wheat starch[J]. *Starch-Stärke*(42(12)), 471-475.

Papanyan Z., Roth D. C., Wittler K., Reimann S., & Ludwig P. D. R. (2013). The dissolution of polyols in salt solutions and ionic liquids at molecular level: ions, counter ions, and

hofmeister effects. *Chemphyschem, 14*(16), 3667-3671.

Guo P., Yu J., Copeland L., Wang S., & Wang S. (2018). Mechanisms of starch gelatinization during heating of wheat flour and its effect on in vitro starch digestibility. *Food Hydrocolloids, 82*, 370-378.

Pérez S., Baldwin P. M., & Gallant D. J. (2009). Chapter 5 - Structural Features of Starch Granules I.pdf. *Starch. Academic Press*, 149-192.

Pérez S., & Bertoft E. (2010). The molecular structures of starch components and their contribution to the architecture of starch granules: A comprehensive review. *Starch - Stärke, 62*(8), 389-420.

Qi Y., Wang N., Yu J., Wang S., Wang S., & Copeland L. (2019). Insights into structure-function relationships of starch from foxtail millet cultivars grown in China. *International Journal of Biological Macromolecules, 155*(15), 1176-1183.

Ren F., Wang J., Luan H., Yu J., Copeland L., Wang S., & Wang S. (2019). Dissolution behavior of maize starch in aqueous ionic liquids: effect of anionic structure and water/ionic liquid ratio. *ACS Omega, 4*(12), 14981-14986.

Ren F., Wang J., Yu J., Xiang F., Wang S., Shujun W., & Les C. (2019). Dissolution of maize starch in aqueous ionic liquids: the role of alkyl chain length of cation and water:ionic liquid ratio. *ACS Sustainable Chemistry & Engineering, 7*(7), 6898-6905.

Rogers R. D., & Seddon e. R. (2003). Ionic Liquids--Solvents of the Future. *Science, 302*(5646), 792-793.

Seoud O. A. E., Koschella A., Fidale L. C., Dorn S., & Heinze T. (2007). Applications of ionic

liquids in carbohydrate chemistry_ A window of opportunities. *Biomacromolecules, 8*(9), 2629-2647.

Tan S. S., & Macfarlane D. R. (2010). Ionic liquids in biomass processing. *Topics in Current Chemistry, 290*, 311-339.

Tang H B. A., Hills B P, et al. (2001). A proton NMR relaxation study of the gelatinisation and acid hydrolysis of native potato starch. *Carbohydrate Polymers, 46*(1), 7-18.

Wang J., Ren F., Yu J., Copeland L., Wang S., & Wang S. (2019). Toward a better understanding of different dissolution behavior of starches in aqueous ionic liquids at room temperature. *ACS Omega, 4*(6), 11312-11319.

Wang S., Chao C., Xiang F., Zhang X., Wang S., & Copeland L. (2018). New insights into gelatinization mechanisms of cereal endosperm starches. *Scientific Reports, 8*(1), 3011.

Wang S., & Copeland L. (2015). Effect of acid hydrolysis on starch structure and functionality: a review. *Critical Reviews in Food Science and Nutrition, 55*(8), 1081-1097.

Wang S., Liu H., Gao W., Haixia C., Jiugao Y., & Peigen X. (2006). Characterization of new starches separated from different Chinese yam (Dioscorea opposita Thunb.) cultivars. *Food Chemistry, 99*(1), 30-37.

Wang S., Wang S., Guo P., Liu L., & Wang S. (2017). Multiscale Structural Changes of Wheat and Yam Starches during Cooking and Their Effect on in Vitro Enzymatic Digestibility. *Journal of agricultural and food chemistry, 65*(1), 156-166.

Wang S., Yu J., Gao W., Pang J., Liu H., & Yu J. (2007). Granule structural changes in native Chinese Yam (Dioscorea opposita Thunb var. Anguo) starch during acid hydrolysis.

Carbohydrate Polymers, 69(2), 286-292.

Wang S., Yu J., & Yu J. (2008). The semi-crystalline growth rings of C-type pea starch granule revealed by SEM and HR-TEM during acid hydrolysis. *Carbohydrate Polymers, 74*(3), 731-739.

Wang S., Yu J., Yu J., Chen H., & Pang J. (2007). The effect of acid hydrolysis on morphological and crystalline properties of Rhizoma Dioscorea starch. *Food Hydrocolloids, 21*(7), 1217-1222.

Wang S., Zhang X., Wang S., & Copeland L. (2016). Changes of multi-scale structure during mimicked DSC heating reveal the nature of starch gelatinization. *Scientific Reports, 6*, 28271.

Wang Y., Chao C., Huang H., Wang S., Wang S., Wang S., & Copeland L. (2019). Revisiting mechanisms underlying digestion of starches. *Journal of agricultural and food chemistry, 67*(29), 8212-8226.

Wilpiszewska K., & Spychaj T. (2011). Ionic liquids: Media for starch dissolution, plasticization and modification. *Carbohydrate Polymers, 86*(2), 424-428.

Zhang B., Xie F., Shamshina J. L., Rogers R. D., McNally T., Halley P. J., Truss R. W., Chen L., & Zhao S. (2017). Dissolution of starch with aqueous ionic liquid under ambient conditions. *ACS Sustainable Chemistry & Engineering, 5*(5), 3737-3741.

Zhao D., Palaparthi A. D., Huang Q., Fu X., Liu H., & Yu L. (2015). Effects of ionic liquid 1-allyl-3-methylimidazolium chloride treatment on the microstructure and phase transition of cornstarch. *Industrial Crops and Products, 77*, 139-145.